JOURNAL OF Materials CHEMISTRY

Glycometallate surfactants Part 2: non-aqueous synthesis of mesoporous titanium, zirconium and niobium oxides†

Deepa Khushalani,[a] Geoffrey A. Ozin*[a] and Alex Kuperman*[b]
[a]*Materials Chemistry Research Group, Lash Miller Chemical Laboratories, 80 St. George Street, University of Toronto, Toronto, Ontario, Canada M5S 3H6*
[b]*The Dow Chemical Company, Midland, Michigan, USA*

Received 23rd March 1999, Accepted 6th May 1999

Cetyltrimethylammonium glycotitanate(IV), glycozirconate(IV) and glyconiobate(V), $CTA_{1,2}[M(OCH_2CH_2)_3]$ where M = Ti(IV), Zr(IV), Nb(V), have been synthesized under non-aqueous conditions by reacting $Na_{1,2}[M(OCH_2CH_2)_3]$ with CTACl in ethylene glycol. The glycometallates all have a structure based upon an octahedral metal center containing three chelated glycolate ligands. In ethylene glycol all of the $CTA_{1,2}[M(OCH_2CH_2)_3]$ moieties are found to self-assemble into a lamellar mesophase with a structure based upon bilayers of cationic CTA^+ that are charge-balanced by $[M(OCH_2CH_2)_3]^{2-}$ counter-anions. Hydrolysis of the lamellar glycometallate mesophase in ethylene glycol leads to well-ordered hexagonal phases of mesoporous zirconia and niobia but partially ordered for mesoporous titania. In all cases it is found that the extent of condensation–polymerization of the transition metal oxide in the as-synthesized mesoporous materials is insufficient to sustain the integrity of the structure after the surfactant template is removed by a thermal treatment. Structure re-enforcement of the metal oxide framework can however be achieved by silanation post-treatment of the dehydrated mesoporous metal oxide with Si_2H_6 at 100 °C. All of the mesoporous transition metal oxides that emerge from this procedure are found to be extensively polymerized and stable to the removal of surfactant. Moreover, they all contain silica in the structure at levels that are tunable over a much wider range as compared to that previously reported in the literature. The method described in this paper is a novel approach to the synthesis of stable high surface area mesoporous transition metal oxides with an adjustable level of silica incorporation into the structure.

Introduction

Ever since the initial publication by Kresge and co-workers at Mobil on the surfactant-mediated synthesis of various types of mesoporous silica,[1,2] there has been a fervent desire to change the composition of these materials and move away from silica-based structures. The impetus for this is that the new compositions would have applications in catalysis, gas separation, ion-exchange and possibly would display fascinating electronic, optical, magnetic, photochemical and/or electrochemical behavior.

Towards this aim of synthesis of transition metal oxide mesoporous structures, various studies have been performed, especially over the past two years, involving oxides of metals such as titanium, niobium, zirconium and tantalum.[3] Predominantly, the difficulty in the synthesis of such structures arises from a very limited choice of metal oxide precursors that are able to sufficiently interact with the amphiphilic templating aggregate and yet at the same time undergo a condensation–polymerization reaction such that the structural integrity of a product mesoporous material is maintained upon subsequent removal of the template.

Ideally, it has been found that for successful synthesis, the following three conditions have to be fulfilled:[4] (i) the inorganic precursor should have the ability to form polyanions or polycations allowing for multidentate binding to the surfactant, (ii) the polyions should be able to condense into a rigid structure and (iii) a charge density matching between the surfactant and the inorganic species is necessary to control the formation of a particular phase of a transition metal oxide mesostructure.

Thus far the reports that have appeared in the literature have cited numerous aqueous synthetic routes towards formation of transition metal based mesoporous structures. However, the difficulty thus far still remains the formation of thermally stable, porous structures with large surface areas and pore volumes.

In addition to demand for pure mesoporous metal oxides, high surface area stable mesoporous mixed metal oxides are also very desirable materials. Dense phase mixed metal oxides have found extensive applications in optics, ceramics, catalysis and as catalyst supports.[5] In catalysis these materials are found to exhibit high thermal stability, surface acidity and catalytic activity. The primary rationale for this reactivity is that the interaction of the mixed oxides at the molecular level generates new surface sites not found in the pure oxides. The enhanced activity has been linked to unusual oxidation states and coordination geometries of the transition element and in some cases has been facilitated by Brønsted acidity.[6] This is considered to result from charge asymmetry associated with heterometal–oxygen moieties. The unique chemical and physical properties exhibited by mixed metal binary oxides depend on both the composition and the degree of homogeneity. It should be noted here that the synthesis of materials with such heteroatom linkages is not trivial. The difficulty in the synthesis arises because the rates of hydrolysis of the transition metal and silicon (usually the preferred second element) precursors have to be made comparable.[5] This offers a severe limitation since usually the crystalline transition metal oxide phases are readily precipitated as a separate phase if the synthesis is not performed carefully.[7]

With respect to the formation of mixed metal oxide mesoporous materials, several reports over the past few years have offered methods for their synthesis.[8] So far, the majority of the techniques have involved doping the siliceous framework with trace amounts of transition elements through simple aqueous synthetic treatments involving the transition element oxide and/or alkoxide precursors. Some of the elements that have been successfully incorporated are Al, V, Sn, Ti and Ni.[7] Although loadings have been high at the as-synthesized level, upon calcination, however, the loading levels have consistently

†Part 1, preceding paper in this issue.

decreased and in some cases most of the transition element is completely removed from the structure, yielding a separate non-porous dense oxide phase.

Herein a synthetic method is described that is an extension of the non-aqueous route used for the formation of mesoporous silica developed in our laboratory.[9] Using this method, the details of the synthesis of mesostructured Ti, Nb and Zr oxide materials are presented. These materials are thermally stable and can be obtained as mixed titanium–silicon, niobium–silicon and zirconium–silicon mesoporous oxides in a wide range of elemental compositions.

Mesoporous titanium oxide–CTABr composites

The use of glycolate complexes of titanium in the synthesis of mesoporous silica–titania is an important extension of our previously reported work on the non-aqueous synthesis of mesoporous silicas using glycosilicate(IV)–surfactant composites as elementary structure building blocks.[9] A publication by Gainsford and co-workers on the synthesis of a sodium glycotitanate(IV) complex in which titanium was six-coordinate provided the impetus for this research.[10] The sodium glycotitanate(IV) complex is related to the sodium glycosilicate(IV) complex of Klinowski and co-workers[11] and Laine and co-workers.[12] The structure of the sodium glycotitanate(IV) complex is shown in Fig. 1. The compound was synthesized using titanium isopropoxide in ethylene glycol in the presence of sodium hydroxide. It crystallized under the $C222_1$ space group in which the titanium(IV) center is six-coordinate and two sodium cations provide the charge balance.

Synthesis

Reagents used for the following syntheses included titanium isopropoxide (99.99%, Aldrich), cetyltrimethylammonium bromide (Aldrich), ethylene glycol (99%, Aldrich), sodium hydroxide (Aldrich) and disilane (Johnson Matthey, 98% purity). All reagents were used as supplied. Sodium tris-glycotitanate(IV) was prepared according to the procedure of Gainsford and co-workers.[10] This complex was used for the preparation of the mesoporous titania from the reaction mixture with the following molar composition:

$Na_2Ti(gly)_3$: 36 ethylene glycol : 0.45 CTABr : 2.2 NaOH

Sodium hydroxide and the surfactant were dissolved in ethylene glycol at 80 °C and then $Na_2Ti(gly)_3$ was stirred into the solution. The resulting mixture was aged at 80 °C for 5 days. Then the mixture was cooled and aged at room temperature for 24 hours. The aged mixture was slowly stirred into 200 ml of deionized water and aged for another 3–4 hours at room temperature. This process allowed the formation of a white precipitate which sedimented to the bottom of the flask. The product was recovered by filtration and washed with deionized water.

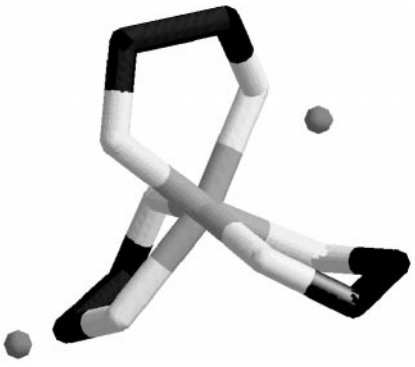

Fig. 1 Structure of sodium tris-glycotitanate(IV).

Results and discussion

The powder X-ray diffraction pattern of the final product is shown in Fig. 2. It can be seen that only one intense peak is observable with a *d*-spacing corresponding to *ca.* 50 Å. This peak appears to have a broad tail that extends up to at least 10° 2θ. It should be noted that peaks attributable to either anatase or rutile (the two commonly occurring polymorphs of titanium dioxide) are not visible in the PXRD pattern of the as-synthesized phase (the rutile peak does, however, appear upon thermal removal of the template). Fig. 3a displays a SEM micrograph of the as-synthesized material. A spherical/globular morphology of the product is apparent. A TEM image of the product is shown in Fig. 3b. Although a distinct hexagonal pattern is not observed, a definite mesoscale patterning is apparent, albeit a partially ordered one. The centre-to-centre distance, calculated from the repetitive pattern, is determined to be about 46 Å, while the wall thickness of the material is estimated to be *ca.* 5–10 Å. These observations are consistent with the PXRD result and from here onwards the phase synthesized is referred to as a mesoporous titanium oxide–CTABr composite.

Fig. 4 displays the TGA weight loss and derivative curve corresponding to the as-synthesized mesoporous material. It is immediately obvious that there is only one major thermal event, at *ca.* 277 °C, however other minor thermal events are also detectable during the ramp between room temperature and 800 °C. The first minor very broad transition is centered at about 100 °C and can be attributed to the loss of adsorbed water. The second predominant transition occurs at *ca.* 277 °C and is attributed to the loss of the occluded surfactant. There appears, in addition, to be a small shoulder at *ca.* 340 °C. It is attributed to the loss of water that is produced by condensation of the neighboring terminal hydroxyl groups. The combined weight loss is 60 wt.% which corresponds to the total loss of water and the imbibed organic template. The ordering of the surfactant inside the mesostructure was studied further by ^{13}C CP/MAS solid state NMR. Fig. 5 compares the ^{13}C NMR spectrum of CTABr in the as-synthesized mesoporous titanium oxide to that of CTABr inside a hexagonal mesoporous silica (both spectra were acquired under identical conditions). The spectra are quite similar. In particular, there is no significant difference detected in the head group region of the surfactant. Carbons in positions 1 and 2 (see insert in Fig. 5) have similar chemical shifts along with relative intensities and peak widths. This result indicates a similar ordering of the surfactant and interaction with the oxide in both the silica and titania structures, in spite of a slight variation mainly in the relative intensities for the carbons 14,

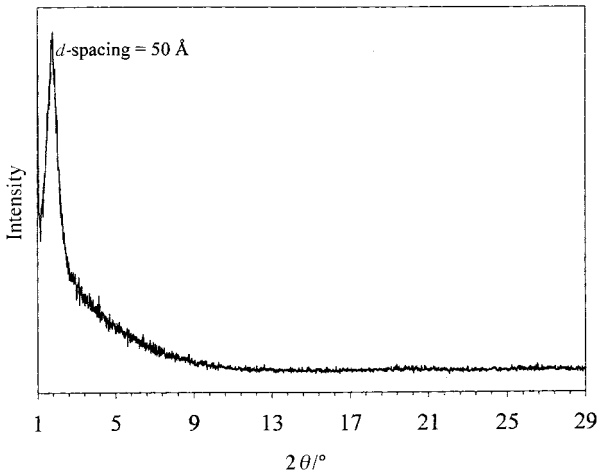

Fig. 2 PXRD pattern of the as-synthesized phase of the mesoporous titanium oxide–CTABr composite.

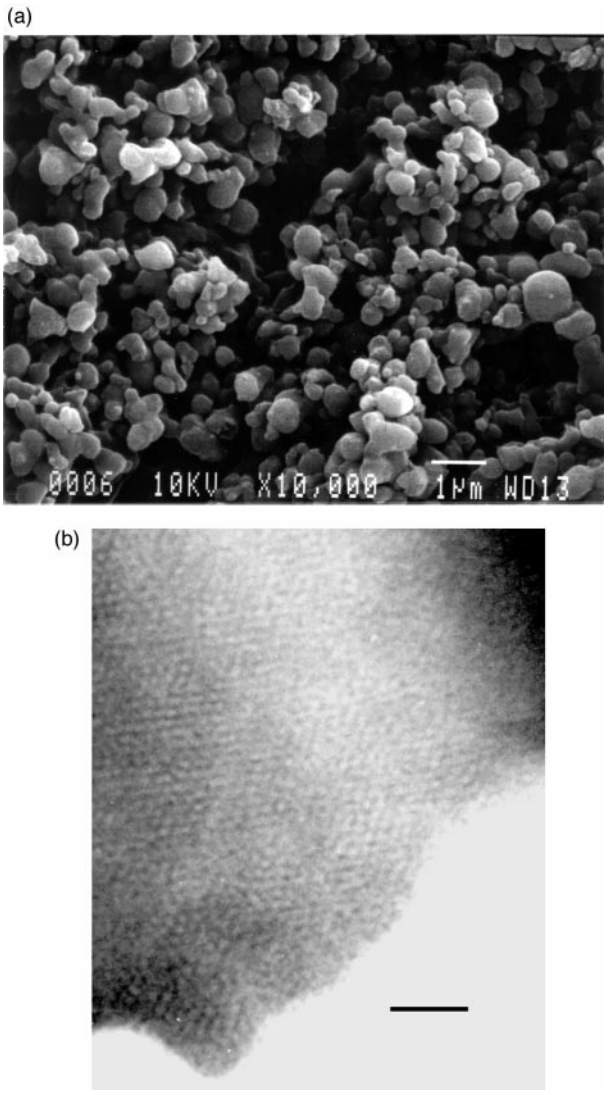

Fig. 3 (a) Scanning electron micrograph of the mesoporous titanium oxide–CTABr composite. (b) Transmission electron micrograph of the synthesized mesoporous titanium oxide. Magnification bar = 30 nm.

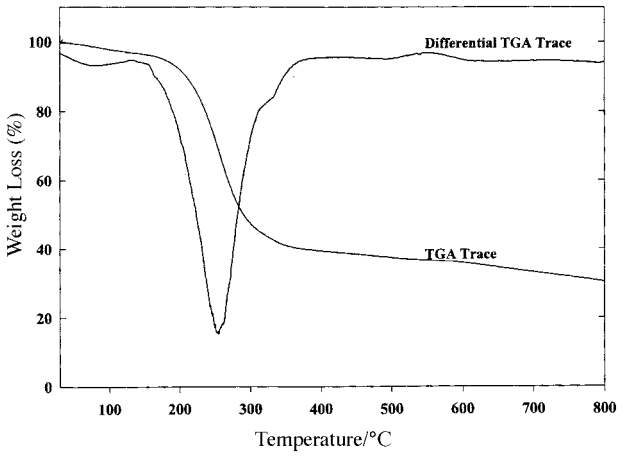

Fig. 4 TGA trace of the mesostructured titanium oxide–CTABr composite.

15 and 16 which are positioned at the end of the alkyl chain and hence are occluded well inside the hydrophobic portion of the assembling aggregate.

The nature and structure of the mesoporous titania were studied closely through vibrational (FT-IR, Raman) and X-ray photoelectron (XPS) spectroscopy. Fig. 6 displays the FT-IR spectrum of the mesoporous titania. Along with the expected vibrational bands for the CTA^+ cation, two ethylene glycol modes are also apparent. This suggests that either the hydrolysis of the starting $[Ti(gly)_3]^{2-}$ complex is incomplete upon the addition of water or a small amount of ethylene glycol is occluded in the structure. Concerning the vibrational modes corresponding to the oxide structure, a broad poorly resolved band is apparent between 400 and 850 cm^{-1}. Since the structure is believed to consist of entirely titanium and oxygen species (with a few glycol pendant groups), it is logical to conclude that the band is inhomogeneously broadened due to slightly different microenvironments of titanium. The same

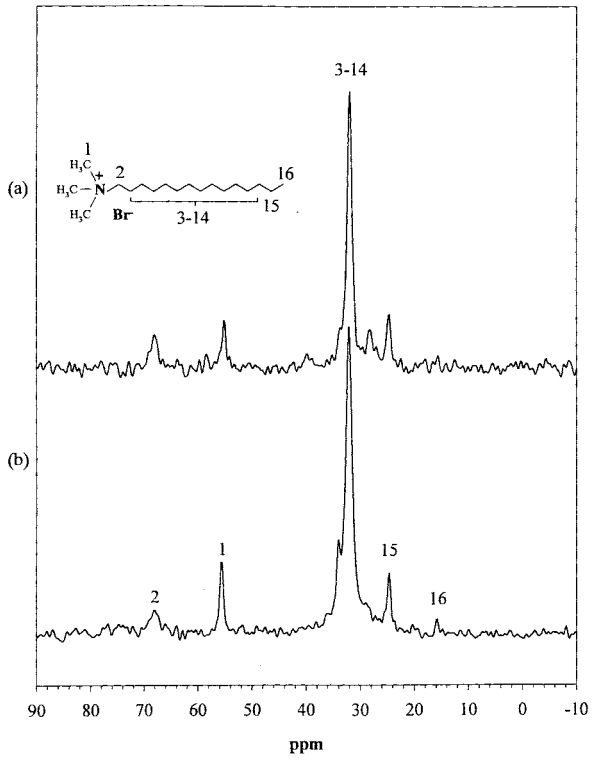

Fig. 5 ^{13}C CP/MAS NMR with proton decoupling of (a) mesoporous silica and (b) mesoporous titanium oxide–CTABr composite. The spectra were acquired on a 200 DSX Bruker spectrometer with a $\pi/2$ width of 4.5 m, contact time of 1 μs, recycle delay of 10 s, 1000 scans and a spinning speed of 5 KHz.

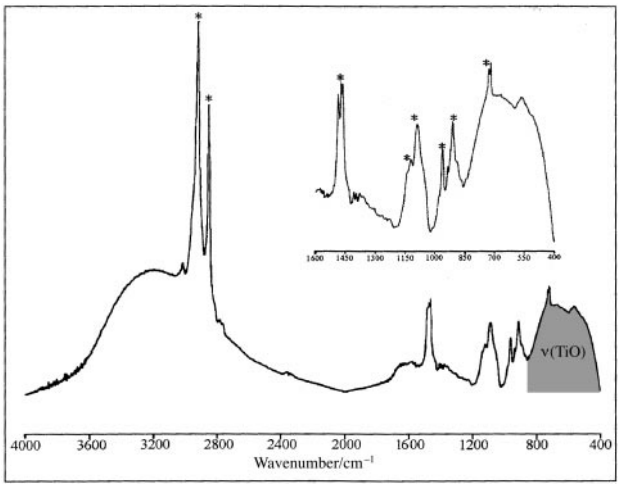

Fig. 6 FT-IR spectrum of the mesoporous titanium oxide–CTABr composite. *, Vibrational modes corresponding to ethylene glycol and CTABr.

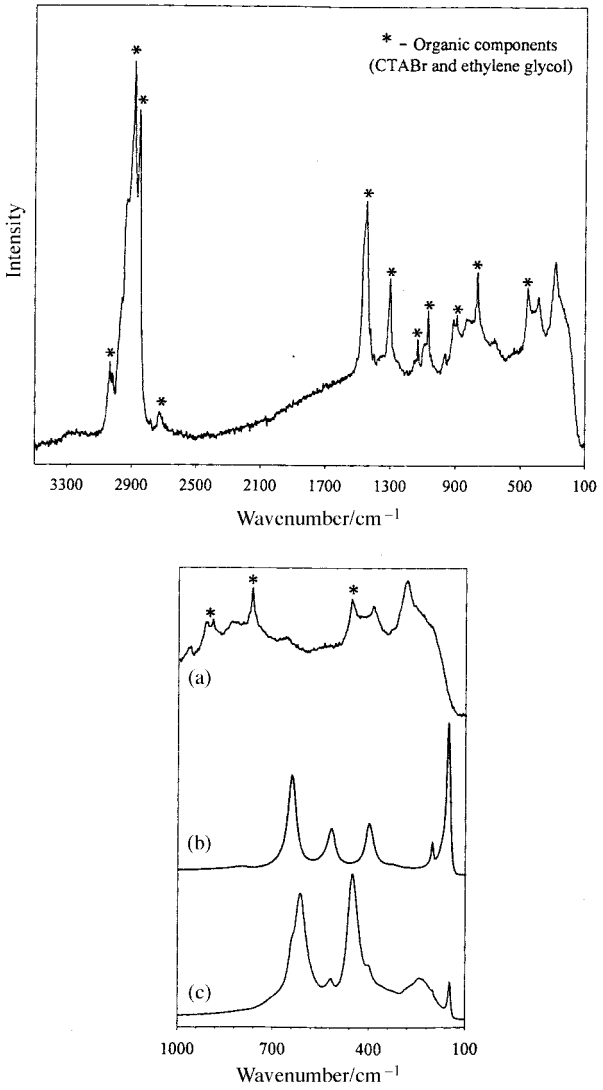

Fig. 7 (Top) FT-Raman spectra of the mesoporous titanium oxide–CTABr composite. (Bottom) Comparison of the low wavenumber end of this spectrum (a) with those of anatase (b) and rutile (containing 2% anatase impurity)(c).

broadening is observed in the spectra of titanium glasses and reflects the amorphous character of these structures.

Additional structural information was obtained through Raman spectroscopy. Fig. 7 displays the corresponding spectrum along with a comparison to the rutile and anatase polymorphs of titanium dioxide. Since this technique is capable of probing local and long range structure, it is effective in determining the presence of trace amounts of the crystalline polymorphs. It is evident from the spectra that neither rutile nor anatase forms of titanium dioxide are present in the as-synthesized mesoporous titania. The characteristic intense lattice modes at 450 and 150 cm^{-1} were not observed. However, an intense broad background was apparent in the region of 100 to 1000 cm^{-1}. This broad background is due to fluorescence which probably arises as a result of defects present in the structure of mesoporous titania. It is interesting, therefore, to note that both FT-IR and Raman results indicate that the walls of the as-synthesized mesoporous titania are built of a unique, largely amorphous titanium oxide phase. A thermal treatment of the as-synthesized mesoporous titania at 600 °C, which is required for the removal of the organic template from the structure, yields solely the rutile polymorph as indicated by PXRD, IR and Raman spectroscopy.

The mesoporous titania was also characterized by X-ray photoelectron spectroscopy (XPS). Fig. 8 displays the survey

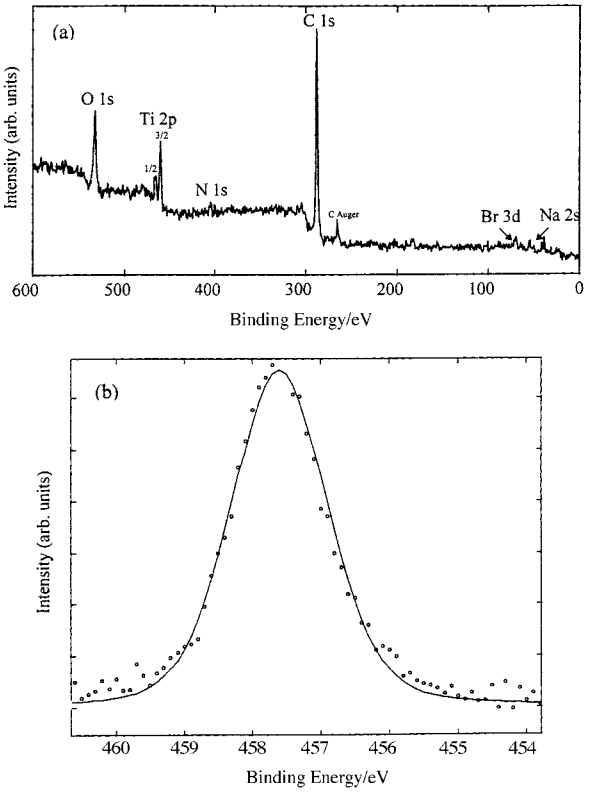

Fig. 8. (a) X-Ray photoelectron spectroscopic survey scan of the surface of the mesoporous titanium oxide–CTABr composite. The peaks have been calibrated with reference to C 1s at 285 eV. (b) A high resolution scan of the Ti $2p_{3/2}$ region showing the fitting profile to yield a peak centered at 457.5 eV with a peak width of 1.7 eV.

XPS spectrum which shows the presence of oxygen, titanium, carbon, nitrogen, sodium and a trace amount of bromine. The presence of these elements was also confirmed by energy dispersive X-ray analyses. Although XPS is solely used as a tool to analyze surfaces (an escape depth of *ca.* 50 Å or less depending on the element) it nonetheless is able to provide some insight regarding the bonding and structure of the material. The primary parameter studied was the coordination of titanium by measuring the binding energy of the Ti 2p core electrons. The Ti $2p_{3/2}$ band was located at 457.5 eV with a peak width of 1.7 eV. This value is 1.7 eV less than the corresponding value for TiO_2 rutile/anatase at 459.2 eV.[13] Although the origin of this shift is not completely clear, the following points need to be considered: (1) the presence of the charge balancing cations in the mesoporous titania, (2) possible change in the coordination number of the titanium in the structure and the nature of oxygen containing ligands (hydroxide, glycolate) as compared to rutile/anatase and (3) increase in the charge density on the titanium centers. The 1.7 eV red shift in the Ti $2p_{3/2}$ peak position indicates that the mesostructured titanium oxide is carrying a net negative charge and is not completely polymerized. The charge is compensated by the CTA^+ and residual Na^+ cations. The XPS results are in good agreement with the IR/Raman data. All three techniques suggest that the as-synthesized mesoporous titania structure has some pendant glycol groups still attached to the titanium centres and a TiO_x wall structure that is built of oxide clusters with a net negative charge that is balanced by a combination of CTA^+ and Na^+ cations.

Mixed titanium–silicon mesoporous oxides

Synthesis

In order to enhance the stability of the structure of the as-synthesized phase and simultaneously allow for the formation

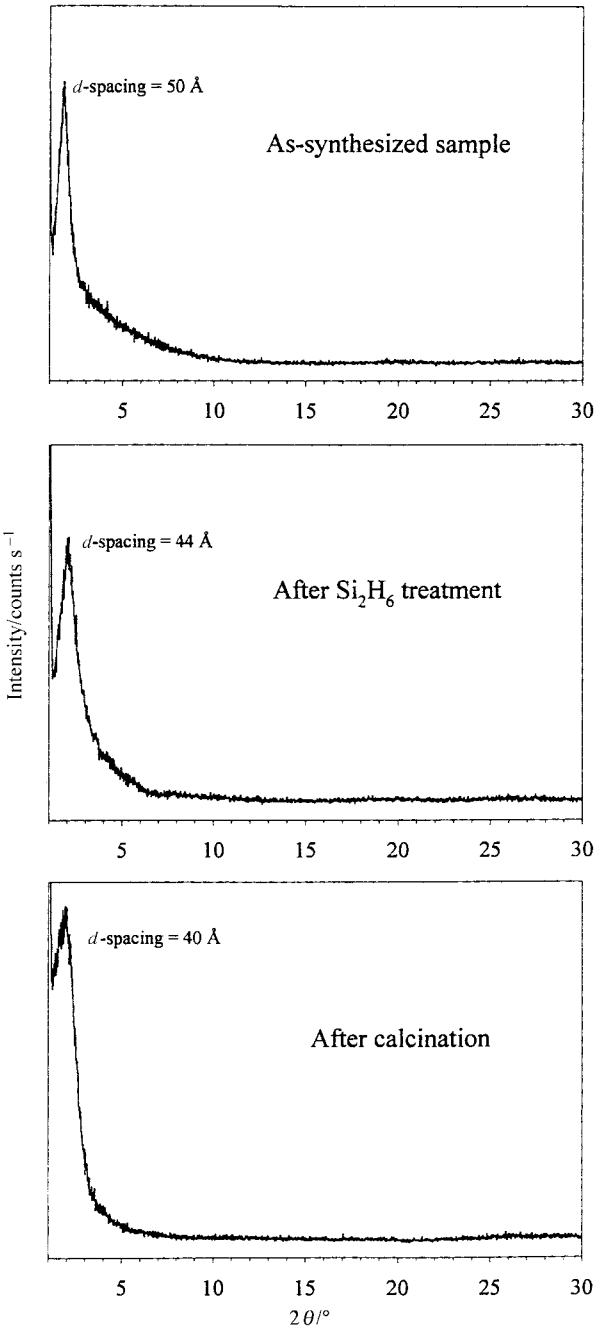

Fig. 9 PXRD patterns of (a) mesoporous titanium oxide–CTABr composite, (b) after Si_2H_6 treatment and (c) after calcination. The ordinate scale is identical for the three patterns.

of a mixed metal oxide, the following procedure was adopted. The mesoporous titanium oxide–CTABr composite was dehydrated under vacuum for 15 hours at 100 °C followed by the gradual exposure to Si_2H_6 at room temperature. The extent of Si_2H_6 incorporation into the mesoporous titania was monitored gravimetrically. Generally, 7 to 15 wt.% of Si_2H_6 was added. Then the cell was sealed and the material was heated to 125 °C and maintained at 125 °C for 48 hours. Any excess of unreacted Si_2H_6 or by-products of the reaction were removed under vacuum. To recover the product, which displayed a black color, it was slowly exposed to air. Upon exposure the color gradually turned white. The calcination procedure of the titania–silica mesocomposite includes heating from 25 °C to 600 °C for 10 hours in air, followed by 1 hour at 600 °C.

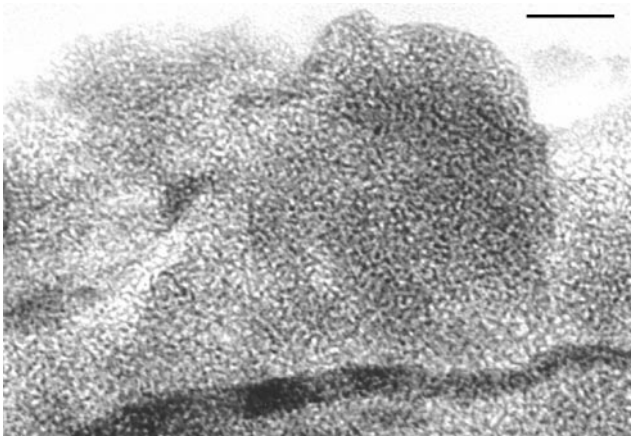

Fig. 10 TEM micrograph of the calcined mixed titanium–silicon mesoporous oxide. The mesopore centre-to-centre distance was estimated to be 40 Å. Magnification bar = 50 nm.

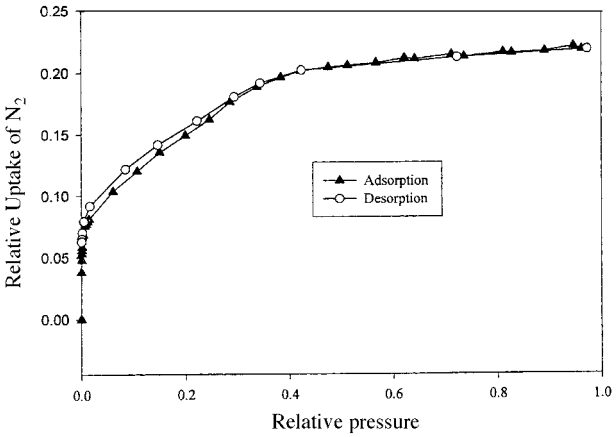

Fig. 11 Nitrogen adsorption and desorption isotherms for the calcined mixed titanium–silicon mesoporous oxide.

Results and discussion

The PXRD patterns for the as-synthesized, disilane treated and calcined materials are shown in Fig. 9. It can be seen that the intensity of the main peak is maintained upon the silanation treatment, however, there is a gradual decrease in the corresponding d_{100}-spacing. More important, however, is the fact that even after calcination the structural integrity is upheld. This directly indicates that Si_2H_6 is able to anchor to hydroxyl groups of the as synthesized dehydrated material, and upon annealing improves the connectivity of the structure to allow retention of its integrity. The PXRD results were verified by transmission electron microscopy, Fig. 10. The micrograph displays a TEM of the calcined material. The presence of a disordered mesostructure is apparent and no other phases are detected. The observed disorder is consistent with the PXRD data, which show the absence of additional indexable peaks in the pattern besides the broadened d_{100} peak. EDX analyses were performed in order to determine the amount of silica deposited and the resulting Ti/Si ratio. The ratios obtained for the product after the initial deposition of disilane were *ca.* 2.5 and after calcination, the value increased to 3. These values can be varied by increasing the loading of Si_2H_6 or the temperature of the thermal treatment that follows. The range of Ti/Si ratios that have been successfully obtained by this method was between 2 and 7.

To probe the porosity of the products, adsorption–desorption studies were performed on the calcined product, Fig. 11. The adsorption–desorption isotherm is of type IV with a slight hysteresis loop. For this isotherm the inflection

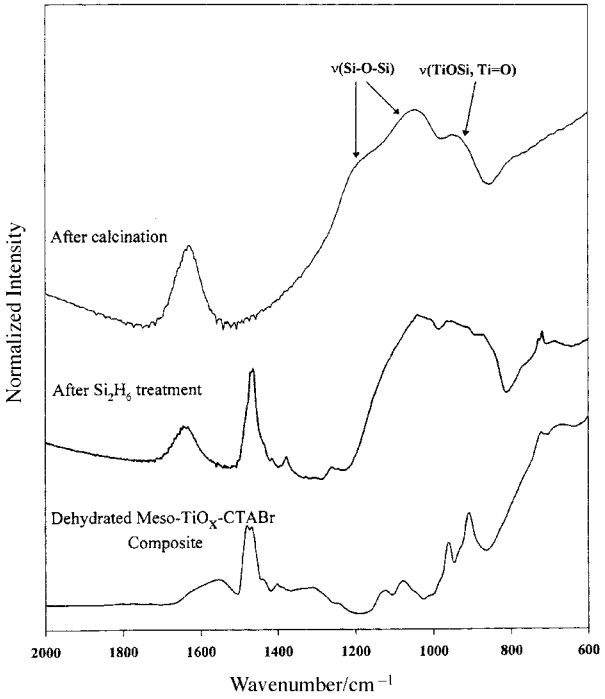

Fig. 12 FT-IR spectra of the mesoporous products obtained after silanation treatment. Note the occurrence of bands in the region of 900 cm^{-1}, signifying the presence of Ti–O–Si linkages and perhaps Ti=O.

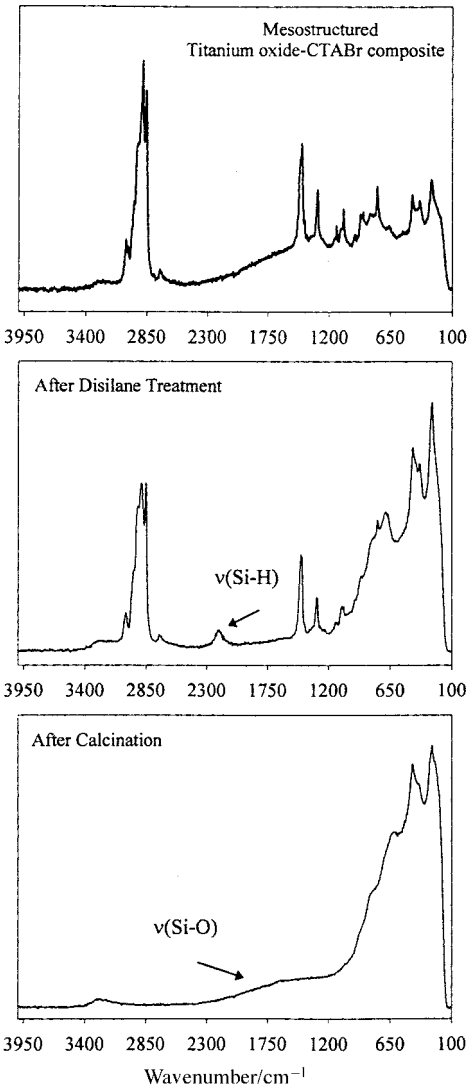

Fig. 13 FT-Raman spectra of the mesoporous product, after silanation and after calcination.

is shallower compared to that of highly ordered mesoporous silica. A shallow inflection is usually characteristic of a broader mesopore size distribution. The pore volume and surface areas obtained by BET[14] analysis of the isotherms were *ca.* 0.3 cm^3 g^{-1} and 420 m^2 g^{-1}. For direct comparison with mesoporous silica this should be done on a mole basis.

^{29}Si MAS NMR was performed to determine the silicon environment in the structure before and after calcination. Upon silanation followed by the annealing treatment, an intense broad peak was detected that covers the region of silicon hydrides (*ca.* −80 ppm) along with the Q_2 and Q_3 silicon signals (*ca.* −90 and 100 ppm, respectively). The peak maximum was located at about 90 ppm. Upon calcination the peak became more intense, broadened and shifted upfield with the peak maximum located at about 100 ppm indicating an increase in the connectivity around silicon sites in the structure. The position of the peak maximum at 100 ppm indicated that silicon sites with Q_3 connectivity are predominant in the calcined structure as compared to much smaller concentrations of Q_2 and Q_4 at *ca.* 90 ppm and 110 ppm respectively. Assuming that titanium second nearest neighbors around the silicon centers as compared to silicon second nearest neighbors do not have a significant effect on the ^{29}Si chemical shifts of Q_n ($Si(OH)_{4-n}O_n$) sites, then the NMR results indicate that most of the silica had been incorporated into the mesoporous titania structure as $(M–O)_3Si–OH$ (M = Ti and/or Si) as opposed to $Si(O–M)_4$. The poor resolution of the ^{29}Si NMR signal can be attributed to the partially ordered nature of the material and/or to the increase in T_2 relaxation time due to the quadrupolar nature of the Ti nucleus in close proximity to the silicon centers.

The changes in the structure of mesoporous silica–titania were also characterized by FT-IR and Raman spectroscopies. The results are shown in Fig. 12 and 13. An important property of the silica–titania materials of this work is that *the Ti/Si ratio in the structure is well above 1*. To date, most of the mixed metal oxides reported in the literature have Ti/Si ratios well below 1. The consequence of this is that certain modes in the IR spectra are enhanced and no longer masked by the intense ν(Si–O–Si) bands that are prevalent in the oxides with large silica content. Previously it was concluded that a prominent band at 960 cm^{-1} in the FT-IR spectra of the framework titanosilicates is an indication of the presence of titanium in the framework in tetrahedral coordination. The band was assigned to an antisymmetric stretch, ν(Si–O–Ti).[15] The origin of this band has, however, been the subject of controversy and it has been demonstrated both theoretically and experimentally that the same signal can be attributed to an isolated structural defect around the silicon centre.[6] In addition, the presence of Ti=O groups in titanosilicates has been hypothesized by the presence of a band in the region of 950 to 1000 cm^{-1}.[15]

In the IR spectrum of mesoporous silica–titania of this work broad bands are observed in the region of 900 to 1300 cm^{-1}. Certainly, as a result of the Si_2H_6 deposition and the subsequent thermal treatment, silica is expected to be an integral part of the structure. This is verified by the presence of the ν_{asym}(Si–O–Si) bands around 1200 and 1050 cm^{-1}. The broadness of these bands indicates the amorphous character of the deposited silica.

Additional information about the mesostructure was achieved from FT-Raman studies, Fig. 13. It can be observed that upon silanation, silicon hydrides are grafted to the material as seen by their stretching frequencies in the region of

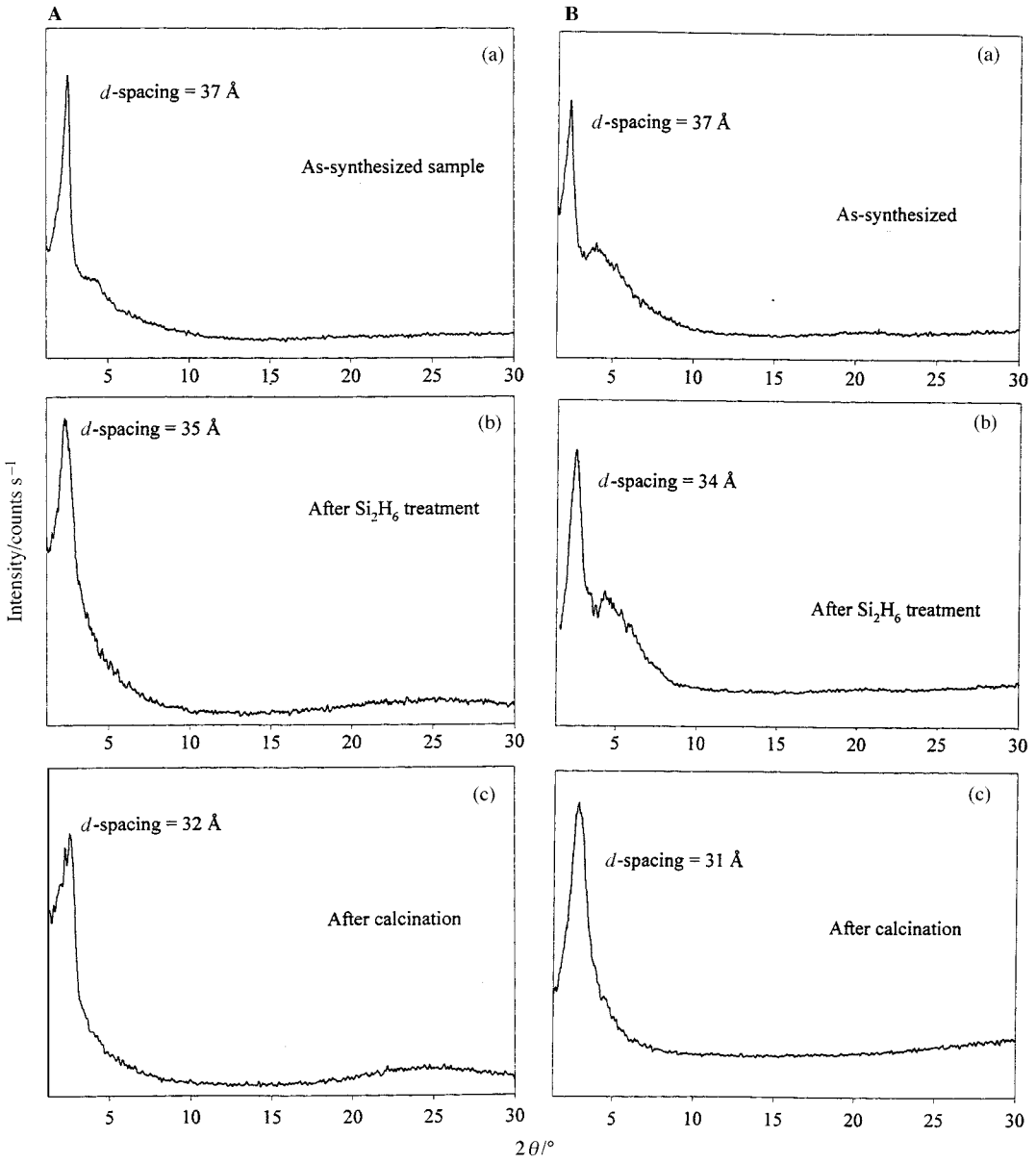

Fig. 14 A, PXRD patterns of (a) the mesoporous niobium oxide–CTABr composite, (b) after Si_2H_6 treatment and (c) after calcination. B, PXRD patterns of (a) the mesoporous zirconium oxide–CTABr composite, (b) after Si_2H_6 treatment and (c) after calcination.

2200 cm^{-1}. These, upon calcination, are removed with the concurrent appearance of an intense broad band in the region of 1200 to 1700 cm^{-1} assigned to ν(SiO), resulting from the amorphous nature of the silica. Upon expansion of the region between 100 and 1200 cm^{-1} distinct peaks at 270 and 450 cm^{-1} along with shoulders at 400, 620, 830 and 940 cm^{-1} can be observed, especially for the sample after calcination. These bands are not characteristic of either the rutile or the anatase phase. The structure can thus be said to consist of a mixed titanium–silicon oxide with Si–O–Ti linkages and the wall structure is completely amorphous.

By X-ray photoelectron spectroscopy studies it was determined that the Ti $2p_{3/2}$ peak position is at 458.5 eV for the silanated product and at 459.1 eV for the calcined material. These values show an increase from the initial value of 457.5 eV and are in agreement with the argument that this change corresponds to a decrease in surface charge of the structure. This can be attributed to an increase in the degree of cross-linking of charged titanium–oxygen species upon silanation and more so upon calcination. The result is a more neutral titanium–silicon oxide mesostructure in which the titanium oxidation state is close to 4+.

Mixed niobium–silicon and zirconium–silicon mesoporous oxides

Synthesis

The same synthetic strategy as in the case of mesoporous titania was employed to create mesoporous niobium and zirconium oxides. Sodium glyconiobate(v) complex was synthesized from a reaction mixture with the following mole ratio of components:

1 $Nb(OC_2H_5)_5$: 30 ethylene glycol : 1 NaOH

The synthetic procedure was identical to that of Gainsford and co-workers.[10] After distillation of the excess glycol, white crystals of sodium glyconiobate(v) were isolated. The crystals were found to be polycrystalline, so that a single crystal XRD structure determination was not possible. Preliminary powder XRD studies resulted in the monoclinic unit cell with a = 13.2 Å, b = 7.84 Å, c = 10.6 Å and β = 111.3 °. The product was used as recovered without further purification. The sodium glycozirconate(IV) complex was synthesized from a reaction

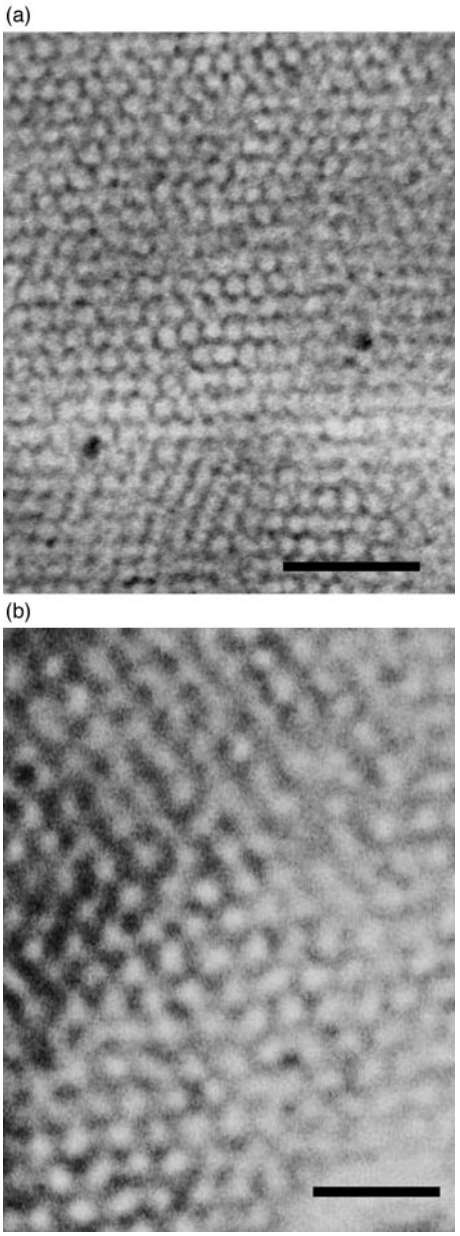

Fig. 15 TEM micrographs of (a) as-synthesized (magnification bar = 25 nm), (b) calcined (magnification bar = 10 nm) mesoporous niobium oxide.

mixture with the following mole ratio of the components:

1 $Zr(OC_2H_5)_4$: 30 ethylene glycol : 2 NaOH

The synthetic procedure was identical to that of Gainsford and co-workers.[10] After distillation of excess glycol, a viscous pale yellow oil remained and was assumed to consist of a polymeric form of sodium glycozirconate. This oil was used directly in the synthesis. The isolated glycometallate complexes were used in the synthesis of mesoporous niobium and zirconium oxides. The mesoporous materials were synthesized from reaction mixtures of the following molar compositions:

1 Nb(Zr) glycolate complex : 40 ethylene glycol :

0.5 CTABr : 1 NaOH

The remainder of the procedure was similar to that for titanium as mentioned above. The only difference was that the hydrolysis was performed in a solution of pH 2 (acidified with HCl). The silanation treatment of the recovered products was identical to that of the mesoporous titanium oxide–CTABr composite.

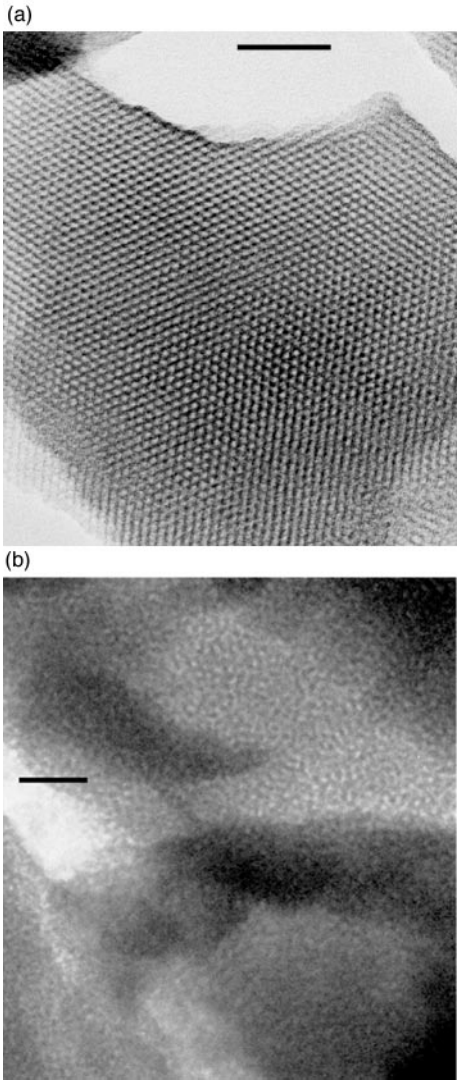

Fig. 16 TEM micrographs of (a) as-synthesized (magnification bar = 38 nm), (b) calcined (magnification bar = 21 nm) mesoporous zirconium oxide.

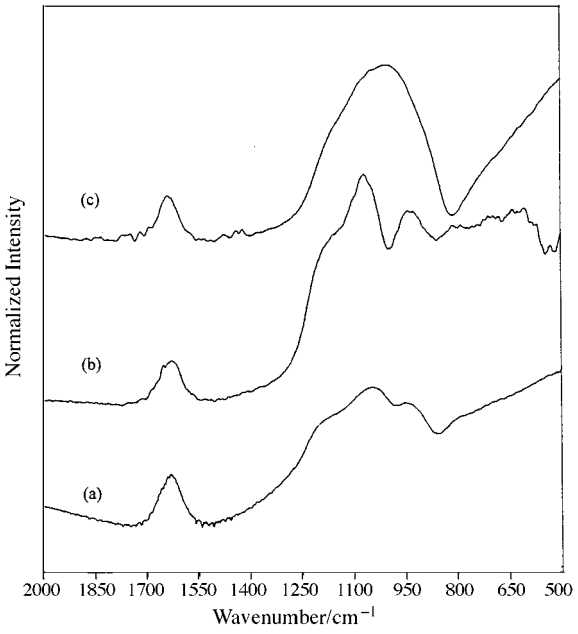

Fig. 17 FT-IR spectra of calcined mesoporous products obtained after silanation treatment: (a) titanium–silicon oxide, (b) niobium–silicon oxide, (c) zirconium–silicon oxide.

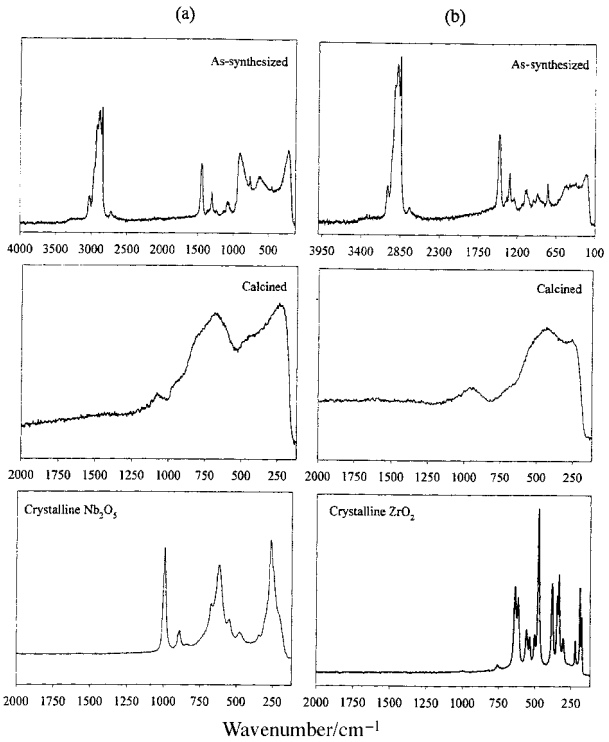

Fig. 18 FT-Raman spectra of mesoporous (a) niobium oxide and (b) zirconium oxide after synthesis, calcination and comparison to a crystalline oxide phase.

Results and discussion

The PXRD patterns of the products of the synthesis and silanation are shown in Fig. 14. Just as in the case of the mesoporous titanium oxide–CTABr composite, a broad peak is detected with a tail extending to 10° 2θ. For the niobium oxide sample, after calcination the *d*-spacing was found to decrease to *ca.* 32 Å and EDX analysis showed that the elemental Nb/Si ratio could be varied between 1.5 and 3. For the zirconium oxide sample, after calcination the *d*-spacing was found to decrease to *ca.* 31 Å and the Zr/Si ratio could be varied between 1.5 and 3. The results of TEM studies performed with these materials are shown in Fig. 15 and 16. After the silanation and calcination treatments, especially in the case of the zirconium oxide sample, the decrease in structural order is quite apparent, and a partially ordered mesoporous structure results as compared to the as-synthesized material. The mesopore centre-to-centre distances calculated from TEM images of the structures are in good agreement with the PXRD data. Argon adsorption studies performed with the calcined samples gave a BET surface area of 180 m^2 g^{-1} for mesoporous mixed niobium–silicon oxide sample while for the mixed zirconium–silicon oxide sample, the BET surface area was 277 m^2 g^{-1}. For direct comparison with mesoporous silica this should be done on a mole basis. In addition to mesoporosity, some textural porosity was also detected in the sample according to the adsorption studies. This type of porosity is usually associated with adsorption into voids that are created by aggregation of very small particles.[16]

The FT-IR spectra of the calcined products are shown in Fig. 17. For the mixed zirconium–silicon oxide sample out of several possible framework vibrational modes in the region of 400 to 1200 cm^{-1} only a broad band centered at 1000 cm^{-1} is visible. However, for the mixed niobium–silicon oxide sample, in addition to a broad band below 800 cm^{-1}, distinct bands at 1200, 1075 and 950 cm^{-1} are detectable. These can be assigned to asymmetric stretching vibrations of Si–O–Si. The band at 950 cm^{-1} can be attributed to the presence of highly but not fully polymerized silica. FT-Raman spectra (Fig. 18), also confirmed the amorphous nature of the wall structure and the absence of crystalline impurities in the final products for both the niobium- and zirconium-based mesoporous oxides. Structural details for both materials can not be obtained from the spectra due to large band widths in the spectral region below 1200 cm^{-1}.

Conclusion

A non-aqueous synthesis of novel mesoporous transition metal oxide and mixed silica–transition metal oxide materials is described. At the early stage of the synthesis a layered phase is formed which consists of a cationic surfactant bilayer assembly charge-balanced by hydrolysable and polymerizable glycotitanate(IV), glycozirconate(IV) or glyconiobate(V) counter-anions. The glycometallate mesophase has the dual function of a supramolecular template and a precursor to mesoporous titanium, zirconium and niobium oxide materials. The robustness of the as-synthesized mesoporous titanium, zirconium and niobium oxide materials can be improved by a mild silanation post-treatment, to create materials that are thermally stable and from which organics can be removed by calcination in the 600 °C temperature range. The synthesis procedure yields framework compositions with broadly tunable and unprecedented M : Si ratios. The availability of a range of main group and transition metal glycometallates opens the way to binary, ternary and quaternary mesoporous mixed metal oxide materials with perceived applications in catalysis, separation, fuel and solar cells, batteries, and chemical sensors.

Acknowledgements

G.A.O. is indebted to the Canada Council for the award of an Issac Walton Killam Foundation Research Fellowship (1995–97) that was held during the period of this research. G.A.O. is also deeply grateful to ESTAC and NSERC-IOR for financial support of this research. We would like to thank Dr. N. Coombs for help with both scanning and transmission electron microscopy, Dr. P. Aroca-Oulette for useful discussions regarding NMR and Dr. R. Sodhi of the Biomaterials Department for assistance with X-ray photoelectron spectroscopy.

References

1 C. T. Kresge, M. E. Leonowicz, W. J. Roth, J. C. Vartuli and J. S. Beck, *Nature*, 1992, **359**, 710.
2 J. S. Beck, J. C. Vartuli, W. J. Roth, M. E. Leonowicz, C. T. Kresge, K. T. Schmitt, C. T-W. Chu, D. H. Olson, E. W. Sheppard, S. B. McCullen, J. B. Higgins and J. L. Schlenker, *J. Am. Chem. Soc.*, 1992, **114**, 10834.
3 D. M. Antonelli and J. Y. Ying, *Angew. Chem.*, *Int. Ed. Engl.*, 1995, **34**, 2014; D. M. Antonelli, A. Nakahira and J. Y. Ying, *Inorg. Chem.*, 1996, **35**, 3126; D. M. Antonelli and J. Y. Ying, *Angew. Chem. Int.*, *Ed. Engl.*, 1996, **35**, 426; D. M. Antonelli and J. Y. Ying, *Chem. Mater.*, 1996, **8**, 874; P. Trens, M. J. Hudson and R. Denoyel, *J. Mater. Chem.*, 1998, **8**, 2147; G. Pacheco, E. Zhao, A. Garcia, A. Sklyarov and J. J. Fripiat, *J. Mater. Chem.*, 1998, **8**, 219; J. Jimenez-Jimenez, P. Maireless-Torres, P. Olivera-Pastor, E. Rodriguez-Castellon, A. Jimenez-Lopez, D. J. Jones and J. Roziere, *Adv. Mater.*, 1998, **10**, 812.
4 A. Sayari and P. Liu, *Microporous Mater.*, 1997, **12**, 149.
5 P. Cousin and R. A. Ross, *Mater. Sci. Eng. A*, 1990, **130** , 119).
6 R. J. Davis and Z. Liu, *Chem. Mater.*, 1997, **9**, 2311.
7 L. Zhufang, J. Tabora and R. J. Davis, *J. Catal.*, 1994, **149**, 117.
8 H. H. Kung and E. I. Ko, *Chem. Eng. J.*, 1996, **64**, 203.
9 D. Khushalani, A. Kuperman and G. A. Ozin, preceding paper in this issue.
10 G. J. Gainsford, T. Kemmitt, C. Lensink and N. B. Milestone, *Inorg. Chem.*, 1995, **34**, 746.
11 B. Herreros, T. L. Barr, P. J. Barrie and J. Klinowski, *J. Phys.*

Chem., 1994, **98**, 4570; B. Herreros, S. W. Carr and J. Klinowski, *Science*, 1994, **263**, 1585.
12 Y. Blohowiak, D. R. Treadwell, B. L. Mueller, M. L. Hoppe, S. Jouppi, P. Kansal, K. W. Chew, C. L. S. Scotto, F. Babonneau, J. Kampf and R. M. Laine, *Chem. Mater*., 1994, **6**, 2177.
13 M. Murata, K. Wakino and S. Ikeda, *J. Electron Spectrosc. Relat. Phenom*., 1975, **6**, 459.
14 K. S. W. Sing, D. H. Everett, R. A. W. Haul, L. Moscou, R. A. Pierotti, J. Rouquerol and T. Siemieniewska, *Pure Appl. Chem*., 1985, **57**, 603; S. Brunauer, P. H. Emmett. and E. Teller, *J. Am. Chem. Soc*., 1938, **60**, 309.
15 A. J. M. De Man and J. Sauer, *J. Phys. Chem*., 1995, **100**, 5025.
16 D. Huybrechts, L. de Bruycker and P. Jacobs, *Nature*, 1990, **345**, 240; P. T. Tanev and T. J. Pinnavaia, *Chem. Mater*., 1996, **8**, 2068.

Paper 9/02291K